## TECHNICAL POINT OF VIEW

# Phantom-Based Standardization Method for ^{123}I-meta-iodobenzylguanidine Heart-to-Mediastinum Ratio Validated by D-SPECT Versus Anger Camera

Shozo Yamashita, PhD[1], Kenichi Nakajima, MD[2], Koichi Okuda, PhD[3], Haruki Yamamoto, BS[1],
Takayuki Shibutani, PhD[4], Tatsuya Yoneyama, MD[5], Shiro Tsuji, MD[6], and Kunihiko Yokoyama, MD[6]

© The Japanese Society of Nuclear Cardiology 2023

## Abstract

*Background*: The ^{123}I-metaiodobenzylguanidine heart-to-mediastinum ratios (HMRs) have been standardized between D-SPECT and Anger cameras in a small patient cohort using a phantom-based conversion method. This study aimed to determine the validity of this method and compare the diagnostic performance of the two cameras in a larger patient cohort.

*Methods*: We retrospectively calculated HMRs from early and late anterior-planar equivalent and planar images acquired from 173 patients in 177 studies using D-SPECT and Anger cameras, respectively. The D-SPECT HMRs were cross-calibrated to an Anger camera using conversion coefficients based on previous phantom findings, then standardized to medium-energy general-purpose collimator conditions. Relationships between HMRs before and after corrections were investigated. Late HMRs were classified into four cardiac mortality risk groups and divided into two groups using a threshold of 2.2 to verify diagnostic performance concordance.

*Results*: Correction improved linear regression lines and differences in HMRs among the groups. The overall ratios of perfect concordance were (134 [75.7%] of 177), and higher in groups with very low (49 [80.3%] of 61) and high (51 [86.4%] of 59) HMRs when the standardized HMR was classified according to cardiac mortality risk. That between the systems was the highest (164 [92.7%] of 177) when the HMR was divided by a threshold value of 2.2.

*Conclusions*: Phantom-based conversion can standardize HMRs between D-SPECT and Anger cameras because the standardized HMR provided comparable diagnostic performance. Our findings indicated that this conversion could be applied to multicenter studies that include both D-SPECT and Anger cameras.

Keywords: ^{123}I-meta-iodobenzylguanidine, Anger camera, D-SPECT, Heart-to-mediastinum ratio, Standardization

**Ann Nucl Cardiol 2023; 9 (1): 85–90**

[123]**I-** meta-iodobenzylguanidine (MIBG) has been used to evaluate severity, cardiac mortality risk, prognostic values according to drug treatment, and responses to therapeutic devices for patients with chronic heart failure (CHF) (1, 2). In neurology, ^{123}I-MIBG is considered as a

biomarker of Lewy-body disease, including Parkinson disease and dementia with Lewy-bodies (DLB), because cardiac ^{123}I-MIBG uptake significantly decreases due to neural degeneration (3, 4). Cardiac uptake can be simply quantified using the heart-to-mediastinum ratio (HMR), but it is dependent on

— 86 —  Yamashita et al.
Standardization of HMR Between D-SPECT and Anger Cameras

Ann Nucl Cardiol 2023；9（1）：85–90

region of interest (ROIs) settings, acquisition protocols, and types of camera collimators, all of which could seriously impact diagnostic accuracy (5–8). Since differences in collimators are critically important, a cross-calibration method has been developed to unify HMRs among them (7, 8). All types of collimators need to be converted to medium-energy general-purpose (MEGP) conditions from a methodological viewpoint, which is in accordance with European recommendations (9). Phantom-based correction using linear regression has been established and it is clinically applied.

Dedicated cardiac single-photon emission computed tomography (SPECT) cameras with cadmium-zinc-telluride (CZT) detectors have been widely applied to myocardial perfusion imaging. Cameras with sensitive CZT detectors having high spatial and energy resolution has reduced acquisition times and injection doses without compromising image quality (10). Although the standard output of a CZT camera is a SPECT image, planar equivalent images can be generated that are comparable to planar images derived from Anger cameras. HMRs between CZT and Anger cameras have been cross-calibrated using such images (11–15). A conversion coefficient (CC) has been determined using a phantom in the same way for D-SPECT (Spectrum Dynamics Medical, Caesarea, Israel and Tokyo, Japan) as for the Anger camera. This CC unified HMRs between the two cameras, indicating that the phantom-based conversion was equally applicable to D-SPECT (13). However, only 40 patients were included and diagnostic performance still required clinical confirmation. Therefore, we aimed to verify the validity of the phantom-based conversion method and the concordance of diagnostic performance between the two cameras using a standardized HMR and a larger patient cohort over a period of 6 years.

## Patients and methods

### Patients

This study retrospectively analyzed 173 patients (92 men and 81 women; mean age, $72.8 \pm 10.8$ years) who participated in 177 studies between July 2016 and June 2022. The patients were assessed by ^{123}I-MIBG imaging to diagnose DLB and Parkinson disease (n＝125), as well as heart failure (n＝52). The Institutional Review Board at the Public Central Hospital of Matto Ishikawa approved this study. The need for written informed consent from the patients was waived due to retrospective nature of the study, and because patients were routinely assessed using D-SPECT and Anger cameras at our institute.

### Data acquisition

Early and late images were acquired from patients at 15 min and 3–4 h after being injected with 111 MBq of ^{123}I-MIBG (MyoMIBG; PDRadiopharma Inc., Tokyo, Japan). Data were firstly acquired using an E. CAM Anger camera (Siemens Healthcare GmbH, Erlangen, Germany), then immediately by D-SPECT. Conventional planar images were acquired from supine patients using the Anger camera for 3 min in a $256 \times 256$ matrix using a low-energy high resolution (LEHR) collimator. The energy was centered at 159 keV with a 15% window. Data were acquired for 10 min from seated patients using D-SPECT that comprised nine mobile CZT detectors, each of which provided one elementary two-dimensional (2D) image per angle. Planar-equivalent images (planograms) generated based on all elementary 2D images that shared the same angle were positioned onto one large field of view (FOV) in a virtual plane (11). A 15% asymmetrical energy window was centered at 159 keV (145–169 keV).

### ROI settings and HMR calculations

The HMRs of conventional planar images derived from the Anger camera were calculated using smartMIBG software (PDRadiopharma Inc., Tokyo, Japan) (5). A circular ROI was manually placed to enclose the entire heart region, and a rectangular ROI was automatically drawn on the upper mediastinum. The HMRs on D-SPECT planar equivalent images were calculated using Planar H2M software (Spectrum Dynamics Medical). A similar ROI was manually set on the heart. Thereafter, a mediastinal ROI was set on the highest mediastinal region, although the position was below that of the Anger camera due to the limited vertical FOV of 160 mm. The intra- and inter-observer reproducibility of the manual ROI analyses on D-SPECT was evaluated using 40 late images in preliminary studies. Three observers performed the ROI analyses, and one of them repeated the analyses two weeks later. The intra- and inter-observer reproducibility of HMRs were excellent with the intraclass correlation coefficients of 1.00 and 0.99, respectively.

### Adjustment and standardization of HMR between D-SPECT and Anger cameras

The HMRs from D-SPECT were adjusted to those of the Anger camera with the LEHR collimator as follows:

Adjusted HMR＝CC of Anger camera/CC of D-SPECT × (measured HMR-1) ＋ 1.

The CCs of the Anger and D-SPECT cameras were 0.55 and 0.63, respectively, based on previous findings (13). Details of the methodology with which to calculate CCs are described elsewhere (7, 8, 13).

We converted the HMRs of the Anger and D-SPECT cameras to the MEGP conditions as follows:

Standardized HMR＝0.88/CC of Anger camera or D-SPECT × (measured HMR-1) ＋ 1. The average CC of the MEGP collimator was 0.88 (8).
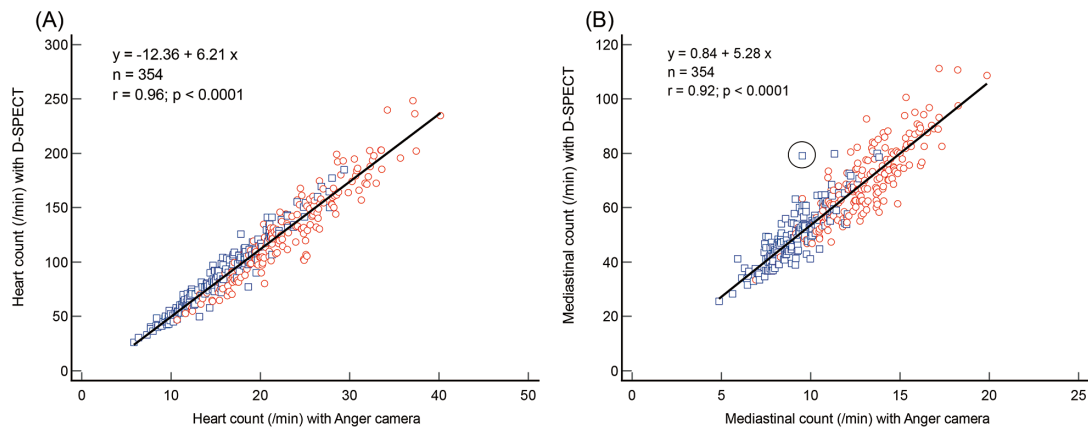
**Figure 1** Relationships of heart (A) and mediastinum (B) counts between D-SPECT and Anger cameras. Circles and squares, early and late counts, respectively. Figure 3 shows dotted circle in (B).

### Statistics

Data are expressed as means ± standard deviation. Linear regression lines and HMR correlations between the D-SPECT and Anger cameras were assessed using the least-squares method and Pearson correlation coefficients, respectively. Agreement of HMRs between the cameras was assessed using Bland-Altman analysis. Paired values were analyzed using paired $t$ tests. Statistical significance was set at $p<0.05$. Late HMRs after standardization was classified according to cardiac mortality risk groups as described (1): $<1.59$ (severely reduced), 1.59–2.02 (moderately reduced), 2.03–2.46 (borderline normal), and $\geq 2.47$ (high normal). Late HMRs were also divided into two groups based on a threshold of 2.2. All data were statistically analyzed using MedCalc v. 20.218 (MedCalc Software Ltd., Ostend, Belgium).

## Results

### Cardiac and mediastinal counts

The heart and mediastinum counts of D-SPECT were approximately 5 times higher than those of Anger camera. Correlations between the cameras were excellent for cardiac ($r=0.96$, $p<0.0001$) and mediastinal counts ($r=0.92$, $p<0.0001$; Figure 1). However, a few outliers had extremely high mediastinum counts on D-SPECT images (Figure 1B)

### HMR before and after corrections

The original HMR was significantly higher for D-SPECT, than the Anger camera images ($1.78 \pm 0.49$ vs. $1.71 \pm 0.36$; $p<0.0001$). The difference in the HMRs was reduced when the HMR from D-SPECT was adjusted to the Anger camera conditions ($1.68 \pm 0.43$) or the standardized HMR was adjusted to MEGP conditions (D-SPECT vs. Anger, $2.09 \pm 0.69$ vs. $2.13 \pm 0.57$), but the significant differences in the HMRs between the two systems persisted after correction ($p=0.0022$).

The linear regression line was improved and close to ideal

($y=x$) when the HMR was converted to LEHR collimator conditions ($y=-0.25+1.13x$, $r=0.94$, $p<0.0001$; Figure 2B), compared with the original HMR conditions ($y=-0.43+1.29x$, $r=0.94$, $p<0.0001$; Figure 2A). The linear regression line was similarly improved after standardization ($y=-0.32+1.13x$, $r=0.94$, $p<0.0001$; Figure 2C).

Although the difference in the original HMR between D-SPECT and Anger cameras had a slight fixed error (mean difference, 0.07; 95% confidence interval (CI) 0.05 to 0.09; Figure 2D), it was reduced when the HMR was adjusted to the LEHR conditions (mean difference, -0.03; 95% CI, -0.04 to -0.01; Figure 2E) or standardized to MEGP conditions (mean difference, -0.04; 95% CI, -0.07 to -0.01; Figure 2F). Proportional errors were similarly improved after corrections, although it statistically persisted ($p=0.0022$; Figure 2E and F).

Figure 3 shows an image from a patient with an extremely low HMR on D-SPECT, compared with Anger camera images. When the mediastinal ROI was reset similarly to D-SPECT, the standardized HMR of the Anger camera decreased and closely matched that of D-SPECT.

### Concordance of diagnostic performance after standardization

Table 1 shows the concordance of late HMR between the two systems when the standardized HMR was classified according to cardiac mortality risk. The rate of perfect concordance was high (134 [75.7%] of 177) particularly in the severely reduced (49 [80.3%] of 61) and high normal (51 [86.4%] of 59) groups. In the mismatched cases, 42 [97.7%] of 43 belonged to the only one group upper or lower than the group classified into the D-SPECT HMR. Table 2 shows the concordance of late HMR when the standardized HMR was divided by a threshold of 2.2. The rate of perfect concordance between the two systems was very high (164 [92.7%] of 177).

— 88 —    Yamashita et al.
Standardization of HMR Between D-SPECT and Anger Cameras
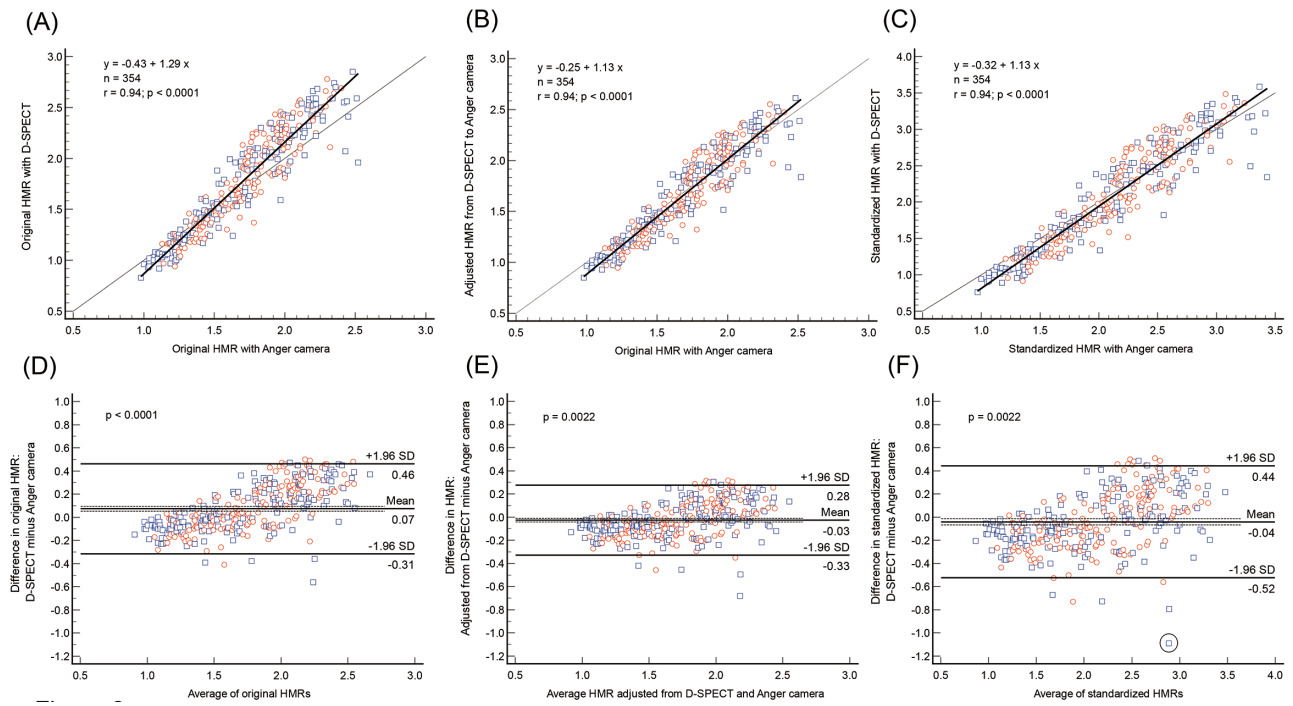
Ann Nucl Cardiol 2023；9（1）：85–90



**Figure 2** Results of linear regression and Bland-Altman analyses of HMRs.

Linear regression and Bland-Altman findings of original HMRs (A and D), D-SPECT HMRs adjusted to Anger camera (B and E), and standardized HMR (C and F) conditions. Dotted lines: (A–C), identity (D–F), 95% CI of mean difference among HMRs. Circles and squares, early and late HMRs, respectively. Figure 3 shows dotted circle in (F).

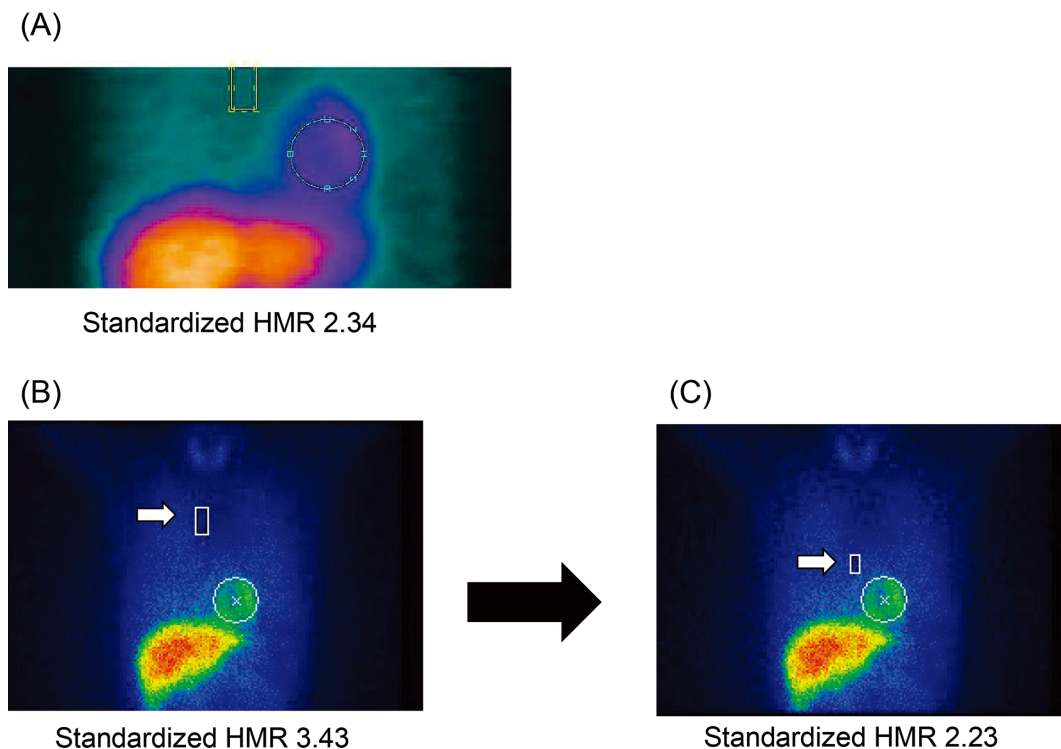CI, confidence interval; HMR, heart-to-mediastinum ratio.



**Figure 3** Images from patient with largest differences in late HMR between two cameras. Settings for D-SPECT images (A), and initial (B) and reset (C) mediastinum ROIs in Anger camera images. White arrow, mediastinum ROI.

HMR, heart-to-mediastinum ratio; ROI, region of interest.

**Table 1** Concordance between cardiac mortality risk groups classified using late HMR

| Anger camera vs. D-SPECT | Severely reduced (<1.59) | Moderately reduced (1.59–2.02) | Borderline normal (2.03–2.46) | High normal (≥2.47) | Group total | Total |
|---|---|---|---|---|---|---|
| Severely reduced (<1.59) | 49 (80.3%) | 12 (19.7%) | 0 | 0 | 61 | |
| Moderately reduced (1.59–2.02) | 0 | 19 (67.9%) | 8 (28.6%) | 1 (3.6%) | 28 | 177 |
| Borderline normal (2.03–2.46) | 0 | 5 (17.2%) | 15 (51.7%) | 9 (31.0%) | 29 | |
| High normal (≥2.47) | 0 | 0 | 8 (13.6%) | 51 (86.4%) | 59 | |

**Table 2** Concordance between values divided by late HMR threshold of 2.2

| Anger camera vs. D-SPECT | <2.2 | ≥2.2 | Group total | Total |
|---|---|---|---|---|
| <2.2 | 91 (94.8%) | 5 (5.2%) | 96 | 177 |
| ≥2.2 | 8 (9.9%) | 73 (90.1%) | 81 | |

## Discussion

The HMRs have been cross-calibrated between CZT and Anger cameras using relatively small patient populations (11–15). This study compared the diagnostic performance of the two cameras with a larger patient cohort and determined the validity of phantom-based conversion for standardizing HMRs.

### Validity of phantom-based conversion

Linear regression lines and differences between HMRs were improved after correction and corresponded with previous findings (13). However, unlike that study, proportional error persisted after correction, which might be attributable to the following. First, the slope of the linear regression line after correction was slightly higher than the line of identity. Second, a few patients had far lower D-SPECT than Anger camera HMRs. The mediastinal ROI settings might have caused discrepancies. Setting ROIs in the lower mediastinum due to a narrow vertical FOV resulted in high mediastinal counts and low HMRs.

A proportional error was evident in the analysis of late HMR (p=0.0065). Thus, we investigated whether the differences in standardized HMRs between the cameras impacted clinical diagnoses.

### Concordance of diagnostic performance after standardization

Late HMR is important for diagnosing of CHF and Lewy-body disease (1–4). When the HMR was classified according to cardiac mortality risk, concordance between the cameras was perfect in > 80% of severely reduced or high normal groups, indicating comparable diagnostic performance between very low and high HMRs. The rate of perfect concordance in groups with a moderately reduced or borderline normal HMRs was lower than in those with a severely reduced or high normal HMRs. However, since most mismatches were found in one group above or below that classified into the D-SPECT HMR, the discordances did not significantly impact diagnosis. When the HMR was classified by a threshold of 2.2, which is applied in neurology to differentiate Alzheimer dementia and DLB (16), the HMR concordance between the cameras was>90%. These findings indicated equivalent diagnostic accuracy between the two systems from a neurological perspective.

This study has some limitations. We calculated the CC based on phantom experiments, whereas body size, ^{123}I-MIBG distribution, and scatter from outside the FOV can widely differ under clinical conditions. Although a phantom can simulate the human body, issues associated with complicated structures might persist. The present study, however, determined that the proposed CC was suitable for cross-calibration purposes between D-SPECT and Anger cameras. Further studies are needed to determine whether the phantom-based conversion method using CC can be applied to the other CZT cameras which do not use planar images. Moreover, the D-SPECT and Anger camera images were respectively acquired from seated and supine patients. The effects of gravity and the respiratory motion of organs due to these different positions were not considered. Manually setting ROIs for D-SPECT together with ROI size could be inconsistent in the clinical setting. Thus, HMRs should be analyzed in the future using software such as smartMIBG. Although the acquisition time of the Anger and D-SPECT imaging was not the same, the interval between the two data sets was only 10 min. A previous study has reported that variation in acquisition time for the late HMRs between 2- and 4-h post-injections did not show significant changes (17). The current study determined the excellent correlations of the heart and mediastinum counts between the Anger and D-SPECT

— 90 — Yamashita et al.
Standardization of HMR Between D-SPECT and Anger Cameras

Ann Nucl Cardiol 2023；9（1）：85–90

cameras, suggesting that the differences in the timing did not significantly affect HMRs.

## Conclusions

We confirmed that the phantom-based conversion can standardize HMRs between D-SPECT and Anger cameras because their diagnostic performances were comparable. Our findings indicated that this conversion could be applied to multicenter studies that include both D-SPECT and Anger cameras.

## Conflicts of interest

K. Nakajima collaborates with Spectrum Dynamics Medical (Caesarea, Israel), Siemens Healthcare (Tokyo, Japan), and PDRadiopharma, Inc (Tokyo, Japan). None of the others has any conflicts of interest to declare.

Reprint requests and correspondence:

Shozo Yamashita, PhD

Division of Radiology, Public Central Hospital of Matto Ishikawa, 3-8 Kuramitsu, Hakusan, Ishikawa 924-8588, Japan

E–mail: y.shozo57@gmail.com

## References

1. Nakajima K, Scholte A, Nakata T, et al. Cardiac sympathetic nervous system imaging with ^{123}I-meta-iodobenzylguanidine: Perspectives from Japan and Europe. J Nucl Cardiol 2017; 24: 952–60.

2. Verschure DO, Veltman CE, Manrique A, et al. For what endpoint does myocardial ^{123}I-MIBG scintigraphy have the greatest prognostic value in patients with chronic heart failure? Results of a pooled individual patient data meta-analysis. Eur Heart J Cardiovasc Imaging 2014; 15: 996–1003.

3. Slaets S, Van Acker F, Versijpt J, et al. Diagnostic value of MIBG cardiac scintigraphy for differential dementia diagnosis. Int J Geriatr Psychiatry 2015; 30: 864–9.

4. Nakajima K, Yamada M. ^{123}I-Meta-iodobenzylguanidine sympathetic imaging: Standardization and application to neurological diseases. Chonnam Med J 2016; 52: 145–50.

5. Okuda K, Nakajima K, Hosoya T, et al. Semi-automated algorithm for calculating heart-to-mediastinum ratio in cardiac Iodine-123 MIBG imaging. J Nucl Cardiol 2011; 18: 82–9.

6. Okuda K, Nakajima K, Sugino S, et al. Development and validation of a direct-comparison method for cardiac ^{123}I-metaiodobenzylguanidine washout rates derived from late 3-hour and 4-hour imaging. Eur J Nucl Med Mol Imaging 2016; 43: 319–25.

7. Nakajima K, Okuda K, Matsuo S, et al. Standardization of metaiodobenzylguanidine heart to mediastinum ratio using a calibration phantom: Effects of correction on normal databases and a multicentre study. Eur J Nucl Med Mol Imaging 2012; 39: 113–9.

8. Nakajima K, Okuda K, Yoshimura M, et al. Multicenter cross-calibration of I-123 metaiodobenzylguanidine heart-to-mediastinum ratios to overcome camera-collimator variations. J Nucl Cardiol 2014; 21: 970–8.

9. Flotats A, Carrió I, Agostini D, et al. Proposal for standardization of ^{123}I-metaiodobenzylguanidine (MIBG) cardiac sympathetic imaging by the EANM Cardiovascular Committee and the European Council of Nuclear Cardiology. Eur J Nucl Med Mol Imaging 2010; 37: 1802–12.

10. Agostini D, Marie PY, Ben-Haim S, et al. Performance of cardiac cadmium-zinc-telluride gamma camera imaging in coronary artery disease: A review from the cardiovascular committee of the European Association of Nuclear Medicine (EANM). Eur J Nucl Med Mol Imaging 2016; 43: 2423–32.

11. Bellevre D, Manrique A, Legallois D, et al. First determination of the heart-to-mediastinum ratio using cardiac dual isotope (^{123}I-MIBG/^{99m}Tc-tetrofosmin) CZT imaging in patients with heart failure: the ADRECARD study. Eur J Nucl Med Mol Imaging 2015; 42: 1912–9.

12. Nakajima K, Okuda K, Matsuo S, Agostini D. The time has come to standardize ^{123}I-MIBG heart-to-mediastinum ratios including planar and SPECT methods. Eur J Nucl Med Mol Imaging 2016; 43: 386–8.

13. Nakajima K, Okuda K, Yokoyama K, et al. Cross calibration of ^{123}I-meta-iodobenzylguanidine heart-to-mediastinum ratio with D-SPECT planogram and Anger camera. Ann Nucl Med 2017; 31: 605–15.

14. Shibutani T, Nakajima K, Yoneyama H, et al. The utility of heart-to-mediastinum ratio using a planar image created from IQ-SPECT with Iodine-123 meta-iodobenzylguanidine. J Nucl Cardiol 2021; 28: 2569–77.

15. Blaire T, Bailliez A, Ben Bouallegue F, Bellevre D, Agostini D, Manrique A. Determination of the heart-to-mediastinum ratio of ^{123}I-MIBG uptake using dual-isotope (^{123}I-MIBG/^{99m}Tc-tetrofosmin) multipinhole cadmium-zinc-telluride SPECT in patients with heart failure. J Nucl Med 2018; 59: 251–8.

16. Nakajima K, Okuda K, Komatsu J. What does diagnostic threshold mean? Deterministic and probabilistic considerations. J Nucl Cardiol 2021; 28: 1702–6.

17. Dimitriu-Leen AC, Gimelli A, Al Younis I, et al. The impact of acquisition time of planar cardiac ^{123}I-MIBG imaging on the late heart to mediastinum ratio. Eur J Nucl Med Mol Imaging 2016; 43: 326–32.